The Astrophysical Journal, 702:1171–1178, 2009 September 10 doi:10.1088/0004-637X/702/2/1171

GAMMA-RAY BURST AFTERGLOW PLATEAUS AND GRAVITATIONAL WAVES: MULTI-MESSENGER SIGNATURE OF A MILLISECOND MAGNETAR?

Alessandra Corsi[1,2,3] and Peter Mészáros[2]
[1] Università di Roma "Sapienza" and INFN-Roma, Piazzale Aldo Moro 2, Roma 00185, Italy; alessandra.corsi@roma1.infn.it
[2] Department of Astronomy & Astrophysics, Department of Physics, and Institute for Gravitation and the Cosmos, The Pennsylvania State University, University Park, PA 16802, USA; nnp@astro.psu.edu
[3] IASF-Roma/INAF, Via Fosso del Cavaliere 100, Roma 00133, Italy
Received 2009 May 22; accepted 2009 July 15; published 2009 August 19

ABSTRACT

The existence of a shallow decay phase in the early X-ray afterglows of gamma-ray bursts is a common feature. Here we investigate the possibility that this is connected to the formation of a highly magnetized millisecond pulsar, pumping energy into the fireball on timescales longer than the prompt emission. In this scenario, the nascent neutron star could undergo a secular bar-mode instability, leading to gravitational wave losses which would affect the neutron star spin-down. In this case, nearby gamma-ray bursts with isotropic energies of the order of 10^{50} ergs would produce a detectable gravitational wave signal emitted in association with an observed X-ray light-curve plateau, over relatively long timescales of minutes to about an hour. The peak amplitude of the gravitational wave signal would be delayed with respect to the gamma-ray burst trigger, offering gravitational wave interferometers such as the advanced LIGO and Virgo the challenging possibility of catching its signature on the fly.

Key words: gamma rays: bursts – gravitational waves – radiation mechanisms: non-thermal

Online-only material: color figures

1. INTRODUCTION

Thanks to *Swift* observations (e.g., Nousek et al. 2006; Zhang et al. 2006), it has now become evident that the "normal" power-law behavior of long gamma-ray burst (GRB) X-ray light curves $F(T) \propto T^{\alpha}$ with $\alpha \sim -1.2$ (where $F(T)$ is the observed flux and T is the observer's time) is often preceded at early times by an initial steep decay ($\alpha \sim -3$), followed by a shallower-than-normal decay ($\alpha \gtrsim -0.5$; see Figure 1). The steep-to-shallow and shallow-to-normal decay transitions are separated by two corresponding break times, 100 s $\lesssim T_{\rm break,1} \lesssim$ 500 s and 10^3 s $\lesssim T_{\rm break,2} \lesssim 10^4$ s. During the shallow-to-normal transition the spectral index does not change, and the decay slope after the break ($\alpha \sim -1.2$) is generally consistent with the standard afterglow model (e.g., Mészáros & Rees 1997; Sari et al. 1998), while the decay slope before the break is usually much shallower. The lack of spectral changes suggests that the shallow phase may be attributed to a continuous energy injection by a long-lived central engine, with progressively reduced activity (for a review see Zhang et al. (2006) and references therein). Recently, Panaitescu & Vestrand (2008) have pointed out that the effects of a late-time energy injection may also be evident in some optical afterglows, around 30–10^4 s after the trigger. Although it is still not clear if a typical "steep-flat-steep" behavior does exist also in short GRB X-ray afterglows, the case of GRB 051221a does fit this scheme remarkably, with a plateau observed right in the middle of the afterglow decay (Soderberg et. al 2006).

Newborn magnetars are among the progenitors proposed to account for shallow decays or plateaus observed in GRB light curves (Dai & Lu 1998; Zhang & Mészáros 2001; Fan & Dong 2006; Yu & Huang 2007). Independent support for this scenario comes from the observation of SN2006aj, associated with the nearby sub-energetic GRB 060218, suggesting that the supernova-GRB connection may extend to a much broader range of stellar masses than previously thought, possibly involving two different mechanisms: a "collapsar" for the more massive stars collapsing to a black hole (BH), and a newborn neutron star (NS) for the less massive ones (Mazzali et al. 2006).

Previous studies aimed at accounting for the afterglow plateaus by invoking a magnetar-like progenitor have assumed that the magnetar's slowdown is dominated by magnetic dipole losses, neglecting the contribution from the emission of gravitational waves (GWs; see Dai & Lu 1998; Fan & Dong 2006; Yu & Huang 2007), or treating them separately as a limiting case for a NS with sufficiently high, constant eccentricity (Zhang & Mészáros 2001). Such studies have shown how magnetars dipole losses may indeed explain the flattening observed in GRB afterglows. In the simplest version of the magnetar scenario, the end of the shallow decay is accompanied by an achromatic break, while several cases of chromatic breaks have *also* been observed (e.g., Panaitescu 2009). Additional mechanisms such as variable microphysical parameters in the fireball shock front (e.g., Panaitescu et al. 2006) or a structured jet model (e.g., Racusin et al. 2008) can be invoked to explain such chromatic breaks. Anyhow, a larger sample of simultaneous optical-to-X-ray observations is needed to firmly assess the achromatic or chromatic behavior of breaks associated with the end of the shallow-decay phase.

In this paper, we investigate in more detail the effects of GW losses on the magnetar's spin-down, and explore quantitatively the signatures which could test whether this is indeed the mechanism at work in the shallow X-ray light curves. Although the precise evolution of a newborn magnetar from birth up to timescales of $\sim 10^3$–10^4 s is difficult to predict or to follow with numerical simulations, here we point out that among the possible evolutionary paths which one may reasonably consider, one plausible and particularly interesting possibility of exploring is that of a newborn NS left over after a GRB explosion, which undergoes a secular bar-mode instability. In this scenario, simple estimates accounting for the most relevant energy loss processes can provide useful insights into the viability of having efficient GW emission associated with a GRB X-ray afterglow plateau. Although these estimates are clearly approximate, since

possible complications like viscosity effects or magnetic field driven instabilities are neglected, they nonetheless allow us to make a first statement on the relevance of the considered process. Moreover, while other scenarios are also possible, the interesting aspect of this particular one is that, on the one hand, GW observations would be facilitated by the presence of an electromagnetic signature to pinpoint the GW signal search, while on the other hand the detection of bar-mode like GWs in coincidence with a GRB X-ray plateau would be a smoking-gun signature of a magnetar pumping energy into the fireball, thus identifying the much-debated plateau mechanism. Given that several alternative scenarios have been invoked to explain the afterglow flattening, which are *not* expected to be associated with GW signals (see e.g., Panaitescu 2008), this would represent a significant step forward in our understanding of GRB physics. Moreover, identifying the presence of a magnetar would confirm that not all GRB explosions necessarily lead to the prompt formation of a BH.

A point of interest for current analyses that GW detectors are carrying out (see e.g., Acernese et al. 2008a; Abbott et al. 2008a, 2008b) is that the scenario described here involves a new class of GW signals, which should be searched for in coincidence with GRBs. These would have a longer duration (10^3–10^4 s) and a different frequency evolution than the type of GW signals currently considered to be possibly associated with GRBs. Moreover, being delayed by minutes to $\lesssim$1 hr with respect to the prompt γ-ray trigger, the GW signal associated with a GRB plateau would offer the challenging possibility of an on-line detection. In light of the fact that the Virgo[4] and LIGO[5] interferometers are now progressing toward their enhanced/advanced configurations, and getting prepared for performing online data analyses, this prospect appears very appealing. It is worth noting that despite a GW signal in coincidence with a GRB plateau could also be searched offline by LIGO or Virgo, an online detection would be highly preferable, since it could serve as a trigger for ground-based optical follow-ups, even if a GRB trigger alert is absent for any reason.

The paper is organized as follows. In Section 2, we briefly describe how GRB afterglow plateaus are modeled in the context of the magnetar model. In Section 3, we review the main processes that can lead to GW emission associated with NS formation. The aim of this section is to show that, among the different mechanisms that can come into play, the high efficiency of the secular bar-mode instability is conducive to producing GW signals which are detectable also from relatively nearby extra-galactic sources. Moreover, it develops on timescales compatible with the observed durations of GRB plateaus. Section 4 describes the general idea and particular aspects of the scenario being explored here, and how it can explain GRB afterglow plateaus with the presence of a magnetar whose spin-down includes both magnetic dipole and bar-mode GW losses. In Section 5, we present the results of our calculations, and in Section 6 we discuss these results, summarizing our conclusions in Section 7.

2. GRB PLATEAUS IN THE MAGNETAR SCENARIO

Although a wide range of GRB progenitors end in the formation of a BH-debris torus system, it has been proposed that some progenitors may lead to a highly magnetized rapidly rotating pulsar (e.g., Usov 1992; Duncan & Thompson 1992; Thompson 1994; Yi & Blackman 1998; Blackman & Yi 1998; Dai & Lu 1998; Kluzniak & Ruderman 1998; Nakamura 1998; Spruit 1999; Wheeler et al. 2000; Ruderman et al. 2000; Levan et al. 2006; Mereghetti 2008; Bucciantini et al. 2009), with such possibility being realized not only in the case of long GRBs associated with collapsars, but eventually also in scenarios relevant for short GRBs, such as NS binary mergers (Dai & Lu 1998, and references therein).

Fast rotating highly magnetized pulsars are among the class of progenitors that may be associated with significant energy input in the fireball for timescales longer than the γ-ray emission, thus being relevant for explaining GRB afterglow plateaus. A detailed analysis of the observable effects linked to the presence of a pulsar pumping energy into the fireball was performed by Zhang & Mészáros (2001), the results of which we briefly recall in what follows.

Consider the general scenario where the GRB is powered by a central engine that emits both an initial impulsive energy input, $E_{\rm imp}$, and a continuous luminosity; the latter varying as a power-law with time, i.e., $L = L_0(\frac{T}{T_0})^q$, where T is the observer's time. This could be the case if the central engine is a pulsar and the initial impulsive GRB fireball is due to ν–$\overline{\nu}$ annihilation or magnetohydrodynamical processes (see e.g., MacFadyen et al. 1999; Popham et al. 1999; Di Matteo et al. 2002; Lee 2005; Oechslin & Janka 2006; Zhang & Dai 2009). In such a case, a self-similar blast wave is expected to form at late times. In a GRB, the timescale T_0 at which the self-similar solution applies is roughly equal to the time for the external shock to start decelerating while collecting material from the interstellar medium (e.g., Sari & Piran 1999). At different times, the total energy into the fireball may be dominated by either the initial impulsive term, or by the continuous injection one, whose contribution will scale as $E_{\rm inj} = \frac{L_0 T_0}{q+1}(\frac{T}{T_0})^{q+1}$. The continuous energy injection term can dominate on the impulsive one for $T \gtrsim T_c$ (where $T_c \gtrsim T_0$ so as to assure that the self-similar solution has already developed when the continuous injection law dominates), if $q > -1$ and $E_{\rm inj}(T_c) \sim E_{\rm imp}$. In the particular case in which $L_0 T_0 \sim E_{\rm imp}$ then $T_c \sim T_0$ and the dynamics is dominated by the continuous injection as soon as the self-similar evolution begins. Generally speaking, one can write $T_c = \max\{T_0, T_0[(q+1)E_{\rm imp}/(L_0 T_0)]^{1/(1+q)}\}$ (Zhang & Mészáros 2001). Note that the continuous injection may, in addition, have another characteristic timescale T_f at which the continuous injection power-law index $q > -1$ switches to a lower value $q < -1$. In such a case, it is only for $T_c < T_f$ that the continuous injection has a noticeable effect on the afterglow light curve (Zhang & Mészáros 2001).

During the energy-injection-dominated phase, the peak flux, peak frequency, and cooling frequency of the synchrotron photons produced by the forward shock (Sari et al. 1998) scale with time as $F_m \propto T^{1+q}$, $\nu_m \propto T^{-(2-q)/2}$, $\nu_c \propto T^{-(q+2)/2}$, respectively (Zhang & Mészáros 2001) that reduce to the standard scalings for $q = -1$ (Sari et al. 1998). In the case of a nearly constant energy supply, i.e., $q \sim 0$, one has $F_m \propto T$, $\nu_m \propto T^{-1}$, $\nu_c \propto T^{-1}$, respectively. These scalings allow one to compute the temporal indices of the afterglow light curve expected during the injection phase. Assuming to be in slow cooling, these are $F_\nu \propto F_m \nu_m^{(p-1)/2} \propto T^{\alpha_1} = T^{(3-p)/2}$ for $\nu_m < \nu < \nu_c$ and $F_\nu \propto F_m \nu_m^{(p-1)/2} \nu_c^{1/2} \propto T^{\alpha_2} = T^{(2-p)/2}$ for $\nu > \nu_c$, where we have indicated with p the power-law index of the electron energy distribution in the shock front (Sari et al.

[4] www.virgo.infn.it
[5] www.ligo.clatech.edu

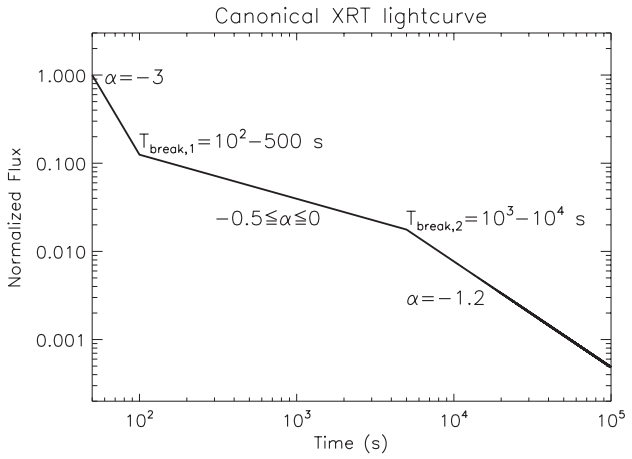

Figure 1. Representation of the typical light-curve behavior observed by *Swift* XRT. The "standard" power-law decay with index $\alpha = -1.2$ is preceded by a flat phase, lasting 10^2–10^4 s, during which the decay index is $\alpha = -0.5$ or flatter (Zhang et al. 2006).

1998). For $2 < p < 4$, one has $0.5 > \alpha_1 > -0.5$ at frequencies $\nu_m < \nu < \nu_c$ and $0 > \alpha_2 > -1$ at $\nu > \nu_c$, to compare with $\alpha \gtrsim -0.5$ observed during GRB afterglow plateaus. In the absence of energy injection, for the standard adiabatic fireball one would have $-3/4 > \alpha_1 > -9/4$ for $\nu_m < \nu < \nu_c$, and $-1 > \alpha_2 > -5/2$ at $\nu > \nu_c$, for the same range of p values. Thus, the presence of a pulsar pumping energy into the fireball at a nearly constant rate is expected to cause a flattening in the typical decay of the afterglow light curve, with $\alpha \gtrsim -0.5$, in agreement with *Swift* observations (see Figure 1).

3. GWs BY NS FORMATION

Gravitational collapse leading to the formation of a NS has long been considered an observable source of GWs. During the core collapse, an initial signal is expected to be emitted due to the changing axisymmetric quadrupole moment. A second part of the GW signal is produced when gravitational collapse is halted by the stiffening of the equation of state above nuclear densities and the core bounces, driving an outward moving shock, with the rapidly rotating proto-neutron star (PNS) oscillating in its axisymmetric normal modes. In a rotating PNS, the nonaxisymmetric processes can also yield to the emission of GWs with high efficiency. Such processes are convection inside the PNS and in its surrounding hot envelope, anisotropic neutrino emission, dynamical instabilities, and secular gravitational-radiation-driven instabilities that we briefly recall in what follows. We refer the reader to e.g., Kokkotas (2008) for a recent, more detailed review.

1. *Convection and neutrino emission.* Two-dimensional simulations of core collapse (Müller et al. 2004) have shown that the GW signal from convection significantly exceeds the core bounce signal for slowly rotating progenitors, being detectable with advanced LIGO for galactic sources. In many simulations, the GW signature of anisotropic neutrino emission has also been considered (Epstein 1978; Burrows & Hayes 1996; Müller & Janka 1997) and estimated to be detectable by advanced LIGO for galactic sources.
2. *Dynamical instabilities.* They arise from nonaxisymmetric perturbations and are of two different types: the classical bar-mode instability and the more recently discovered low-$T/|W|$ bar-mode and one-armed spiral instabilities. In Newtonian stars, the classical $m = 2$ bar-mode instability is excited when the ratio $\beta = T/|W|$ of the rotational kinetic energy T to the gravitational binding energy $|W|$ is larger than $\beta_{\rm dyn} = 0.27$ (Chandrasekhar 1969). It can be excited in a hot PNS a few ms after core bounce, or alternatively a few tenths of seconds later, when the PNS cools due to neutrino emission and contracts further, with β becoming $\gtrsim \beta_{\rm dyn}$ ($\beta \propto 1/R$ during contraction). The instability grows on a dynamical timescale (the time that a sound wave needs to travel across the star) which is about one rotational period, and may last from 1 to 100 rotations depending on the degree of differential rotation (e.g., Baiotti et al. 2007; Manca et al. 2007). If the bar persists for ∼10–100 rotation periods, then even signals from distances considerably larger than the Virgo Cluster are estimated to be detectable. An $m = 1$ one-armed spiral instability has also been shown to become unstable in PNS, provided that the differential rotation is sufficiently strong (with matter on the axis rotating at least 10 times faster than matter on the equator, Centrella et al. 2001; Saijo et al. 2002). In recent simulations of rotating core collapse to which differential rotation was added (Ott et al. 2005), the emitted GW signal reached a maximum amplitude comparable to the core-bounce axisymmetric signal, after ∼100 ms and at a frequency of ∼800 Hz.
3. *Secular instabilities.* At lower rotation rates, a star can become unstable to secular nonaxisymmetric instabilities, driven by gravitational radiation or viscosity. Secular GW-driven instabilities are frame-dragging instabilities usually called Chandrasekhar–Friedman–Schutz (CFS; Chandrasekhar 1970; Friedman 1978) instabilities. Neglecting viscosity, the CFS instability is generic in rotating stars for both polar and axial modes. In the Newtonian limit, the $l = m = 2$ f-mode, which has the shortest growth time of all polar fluid modes ($1\ {\rm s} \lesssim \tau_{\rm GW} \lesssim 7 \times 10^4$ s for $0.24 \gtrsim \beta \gtrsim 0.15$; see Lai & Shapiro 1995), becomes unstable when $\beta \gtrsim 0.14$. The f-mode instability, also referred to as the secular bar-mode instability, is an excellent source of GWs. In the ellipsoidal approximation, Lai & Shapiro (1995) have shown that the mode can grow to a large nonlinear amplitude modifying the star from an axisymmetric shape to a rotating ellipsoid that becomes a strong emitter of GWs until the star is slowed-down toward a stationary state. This stationary state is a Dedekind ellipsoid, i.e., a nonaxisymmetric ellipsoid with internal flows but with a stationary (nonradiating) shape in the inertial frame. During the evolution, the nonaxisymmetric pattern radiates GWs sweeping through the advanced LIGO/Virgo sensitivity window (from 1 kHz down to about 100 Hz), which could become detectable out to a distance of more than 100 Mpc. Two recent hydrodynamical simulations (Shibata & Karino 2004; Ou et al. 2004, in the Newtonian limit and using a post-Newtonian radiation reaction, respectively) have essentially confirmed this picture.
Among axial modes, the $l = m = 2$ r mode is an important member (see e.g., Andersson 1998; Friedman & Morsink 1998; Lindblom et al. 1998; Owen et al. 1998; Lindblom & Owen 2002; Andersson & Kokkotas 2001; Andersson 2003; Bondarescu et al. 2009). If the compact object is a strange star, such instability is predicted to persist for a few 100 yr (at a low amplitude) and, integrating data for a few weeks, could yield to an effective amplitude $h_{\rm eff} \sim 10^{-21}$ for galactic signals, at frequencies ∼700–1000 Hz (Kokkotas 2008).

4. *Other magnetic-field related effects.* Finally, mechanisms different from rotational instabilities can be invoked as GW sources in newborn magnetars. For example, in several scenarios the star's shape may be dominated by the distortion caused by very high internal magnetic fields (e.g., Palomba 2000; Cutler 2002; Arons 2003; Stella et al. 2005; Dall'Osso & Stella 2007; Dall'Osso et al. 2008). GW signals produced by these kind of processes are typically estimated to be detectable by the advanced interferometers up to the Virgo Cluster (i.e., distances of the order of 20 Mpc).

4. THE NS SPIN-DOWN

On the longer afterglow timescales that are of interest for the present work, the energy injection into the fireball by a magnetar eventually surviving after the GRB explosion is expected to be mainly through electromagnetic dipolar emission (Zhang & Mészáros 2001). For what concerns GW losses, in this work we focus on the secular bar-mode instability, given its high efficiency in the production of GWs, and being its characteristic timescale $\tau_{\rm GW}$ compatible with the one of the GRB plateaus (see Sections 3 and 4).

As discussed in the previous section, a collapsing core rotating sufficiently fast is expected to become nonaxisymmetric when β is sufficiently large. Since a new-born NS can be secularly unstable but dynamically stable only if the rotation rate of the pre-collapse core lies in a narrow range, and since during the collapse β increases proportionally to R^{-1}, Lai & Shapiro (1995) considered more likely that the core becomes dynamically unstable ($\beta > \beta_{\rm dyn}$) following the collapse, provided the initial β_i is not too small. On a short dynamical timescale, such NS will evolve toward a nearly axisymmetric equilibrium state, with β decreasing below $\beta_{\rm dyn}$, but possibly remaining above $\beta_{\rm sec}$ (see Lai & Shapiro 1995, and references therein). Due to gravitational radiation, the nearly axisymmetric core (secularly unstable Maclaurin spheroid) will evolve into a nonaxisymmetric configuration (Riemann-S ellipsoid), on a secular dissipation timescale $\sim\tau_{\rm GW}$. While an initial dynamical unstable phase would possibly produce a GW burst during the GRB, the secular evolution takes place on longer timescales, thus being relevant for the shallow phase (100 s $\lesssim T \lesssim 10^4$ s) observed in GRB afterglows (see Figure 1). For this reason, in what follows we focus on the *secular* bar-mode instability. It is worth noting, however, that also the presence of a bar-like GW burst from a *dynamical* bar-mode instability would provide a hint for a magnetar being formed in the GRB explosion. BH formation, in fact, is not expected to lead to strong quadrupole moments (except if it is argued for blobs forming in the infall, see e.g., Kobayashi & Mészáros 2003), and in any case a dynamically unstable magnetar would presumably give rise to a more regular signal.

Fully general relativistic axisymmetric simulations of rotating stellar core collapse in three spatial dimension, performed for a wide variety of initial conditions (rotational velocity profile, equations of state, total mass), indicate that the threshold $\beta = 0.27$ for the onset of the classical dynamical instability is passed if the progenitor of the collapse is: (1) highly differentially rotating; (2) moderately rapidly rotating with $0.01 \lesssim \beta_i \lesssim 0.02$; (3) massive enough (Shibata & Sekiguchi 2005). More recent numerical collapse simulations of rotating stellar iron cores to PNS have also provided an extensive set of post-bounce rotational configurations, allowing studies of the prospects for the development of nonaxisymmetric rotational instabilities. For example, Dimmelmeir et al. (2008) found that the rotational barrier imposed by centrifugal forces prohibits the spin-up necessary for the classical dynamical bar-mode instability, but a large subset of post-bounce models exhibits a β above the secular instability threshold. Based on their results, Dimmelmeir et al. (2008) consider it unlikely that a PNS in nature develops a high-β dynamical instability at or early after core bounce. While many of the PNS could theoretically reach $\beta_{\rm dyn}$ during their subsequent cooling to the final condensed NS (if angular momentum is conserved), it is however considered more likely that the secular instability driven by dissipation or gravitational radiation back-reaction will set in first (Dimmelmeir et al. 2008). Still, three-dimensional simulations are necessary to provide conclusive tests of these predictions.

Under the hypothesis that a secular bar-mode instability does indeed set in, in this work we follow the NS quasi-static evolution under the effect of gravitational radiation according to the analytical formulation given by Lai & Shapiro (1995). Such evolution can in principle be studied using the full dynamical equations of ellipsoidal figures (Chandrasekhar 1969), including gravitational radiation reaction. However, since $\tau_{\rm GW}$ is generally much longer than the dynamical time of the star, the evolution is quasi-static, i.e., the star evolves along an equilibrium sequence of Riemann-S ellipsoids. Differently from what done by Lai & Shapiro (1995), here we add in the energy losses the contribution of magnetic dipole radiation, under the hypothesis that those will not substantially modify the dynamics, but will act speeding up the overall evolution of the bar along the same sequence of Riemann-S ellipsoids that the NS would have followed in the absence of radiative losses. As we are going to show in the following section, dipole losses are nearly constant during the bar evolution so that, according to what discussed in Section 2 for the $q = 0$ case, they can act as a source of continuous energy supply into the fireball, explaining the observed slope of GRB afterglow plateaus.

It is worth noting that in a real situation where magnetic field instabilities and viscosity effects are also present, the relevant timescales may be altered. A secularly evolving bar can last up to a timescale of the order of 10^3 s, as far as viscosity or magnetic field induced instabilities do not substantially modify the dynamics. Viscosity may play a role on the secular evolution when the PNS has cooled to below $\sim$1 MeV (e.g., Lai & Shapiro 1995; Lai 2001). The time required for the pulsar to cool below such temperature was estimated as a few hundreds of seconds by Lai (2001). In the case of a GRB explosion, a less rapid cooling is expected due to continuous in-fall and jet emission (a heating source which was absent in e.g., Lai 2001), so that we may assume that the bar survives at least until the end of the electromagnetic plateau (i.e., $T \sim 10^3$ s). Magnetic effects are notoriously difficult to predict (see e.g., Shibata & Karino 2004), and in general require making heuristic assumptions. In the context of the secular r-mode instability, Rezzolla et al. (2001) have shown that the growth of an initial magnetic field associated with the secular kinematic effects emerging during the evolution of the instability possibly damps the growth of the instability itself. Despite the different context (r-modes), these results do suggest that magnetically driven instabilities may complicate the scenario. In what follows, we explore the quantitative consequences of making the plausible assumption that magnetic instabilities are less efficient at spinning down the bar than GW emission and magnetic dipole losses. Moreover, apart from magnetic braking (spin-down due to dipole losses) which we do consider here, the presence of a magnetic field can influence

the secular evolution in other ways. A magnetic field anchored on the star's surface is in fact perturbed by the instability itself, and this can lead to electromagnetic losses which can enhance the CFS mechanism. For example, in the context of *r*-modes, Ho & Lai (2000) have considered the electromagnetic radiation associated with the shaking of magnetic field lines by the *r*-mode oscillations. This effect has been estimated to be negligible for NS with magnetic field strengths below 10^{16} G. In our case, magnetic field lines anchored on the surface would be distorted by the bar-mode instability. In our treatment, we neglect this effect and include only dipole losses associated with a magnetic field whose flux is conserved on a sphere of radius equal to the mean radius of the ellipsoid.

5. MODELING OF THE NS EVOLUTION

A general Riemann-S ellipsoid is characterized by an angular velocity $\Omega\widehat{e}_3$ of the ellipsoidal figure (the pattern speed) about a principal axis $\widehat{e}_3$, and by internal fluid motions which are assumed to have uniform vorticity $\zeta\widehat{e}_3$ along the same axis (in the frame co-rotating with the figure). Labeling with a_1 and a_2 the principal axes of the ellipsoidal figure in the equatorial plane,[6] and with x_1 and x_2 Cartesian coordinates in such a plane, it can be shown that the fluid velocity in the inertial frame reads

$$\vec{u}_0 = \vec{u} + \Omega(\widehat{e}_3 \times \vec{r}), \tag{1}$$

with

$$\vec{u} = \frac{a_1}{a_2}\Lambda x_2\widehat{e}_1 - \frac{a_2}{a_1}\Lambda x_1\widehat{e}_2, \tag{2}$$

the velocity in the frame co-rotating with the figure (Chandrasekhar 1969), where $\widehat{e}_1$ and $\widehat{e}_2$ are the unit vectors along the Cartesian axes x_1 and x_2; $\vec{r}$ is the position vector; $\times$ indicates the vector product; and

$$\Lambda = -\frac{a_1 a_2}{a_1^2 + a_1^2}\zeta \tag{3}$$

is the angular frequency of the internal fluid motions, i.e., of the elliptical orbits that the particles span around the rotational axis in addition to the pattern motion. The velocity $\vec{u}_0$ is contained in the plain perpendicular to the rotational axis $\widehat{e}_3$, so indicating with $\vec{r}_\perp$ the projection of the position vector $\vec{r}$ in such a plane we can write $\vec{r} = \vec{r}_\perp + x_3\widehat{e}_3$, and $\vec{u}_0 = d(\vec{r}_\perp)/dt + (dx_3/dt)\widehat{e}_3 = d(\vec{r}_\perp)/dt$ (i.e., $dx_3/dt = 0$ since the component of $\vec{u}_0$ along $\widehat{e}_3$ is null). Further, we can write $\vec{u}_0 = (dr_\perp/dt)\widehat{r}_\perp + r_\perp d(\widehat{r}_\perp)/dt = (dr_\perp/dt)\widehat{r}_\perp + r_\perp(\vec{\Omega}_0 \times \widehat{r}_\perp)$, where we have set

$$\vec{\Omega}_0 = \frac{1}{r_\perp}(\widehat{r}_\perp \times \vec{u}_0). \tag{4}$$

Note that $\vec{\Omega}_0$ is defined in such a way that $r_\perp\Omega_0$ gives the component of the particle velocity perpendicular to the polar radius $\vec{r}_\perp$, measured in the inertial frame. However, as underlined above, the motion of fluid particles on the surface can be viewed as the superposition of a circular motion with the pattern frequency Ω, plus an elliptical motion on paths contained on the pattern ellipsoid (resulting in maintaining the pattern fixed). Since the internal fluid motions are ellipses rather than circles, there is an additional component of the velocity parallel to $\vec{r}_\perp$. Using Equation (1), one has

$$\vec{\Omega}_0 = \left[\Omega - \left(\frac{a_2^2 x_1^2 + a_1^2 x_2^2}{r_\perp^2 a_1 a_2}\right)\Lambda\right]\widehat{e}_3. \tag{5}$$

In the frame co-rotating with the pattern, fluid particles on the star's surface move around the rotational axis on ellipses contained in $x_3 = \text{const}$ planes. These ellipses are self-similar to the equatorial one and have the equation

$$\frac{x_1^2}{a_1^2\left(1 - \frac{x_3^2}{a_3^2}\right)} + \frac{x_2^2}{a_2^2\left(1 - \frac{x_3^2}{a_3^2}\right)} = 1. \tag{6}$$

For such fluid particles, $a_2^2x_1^2 + a_1^2x_2^2 = a_1^2a_2^2\left(1 - \frac{x_3^2}{a_3^2}\right)$, and $\langle r_\perp\rangle = \sqrt{a_1 a_2\left(1 - \frac{x_3^2}{a_3^2}\right)}$, so that in one cycle $\left\langle\frac{a_2^2x_1^2 + a_1^2x_2^2}{r_\perp^2 a_1 a_2}\right\rangle = 1$. Thus, in the inertial frame, fluid particles on the star's surface are characterized by an angular frequency

$$\Omega_{\rm eff} = \langle\Omega_0\rangle = \Omega - \Lambda. \tag{7}$$

Since the gravitational radiation reaction acts like a potential force, the fluid circulation along the equator of the star

$$C = \int_{\rm equator} \vec{u}_0 \cdot d\vec{l} = \pi a_1 a_2 \zeta_0, \tag{8}$$

where $d\vec{l}$ is taken along the star's equator, and ζ_0 is the vorticity in the inertial frame, is conserved in the absence of viscosity (Lai et al. 1993). Therefore, the NS will follow a sequence of Riemann-S ellipsoids with constant circulation. Treating the NS as a polytrope of index n (Chandrasekhar 1939), total mass M, and indicating with R_0 the radius of the nonrotating, spherical equilibrium polytrope with same mass M, one has (Lai & Shapiro 1995)

$$\bar{\mathcal{C}} = \frac{\mathcal{C}}{\sqrt{GM^3R_0}} = -\frac{Mk_nC}{5\pi\sqrt{GM^3R_0}}, \tag{9}$$

where G is the gravitational constant; k_n is a constant which depends on the index n of the considered polytrope (see e.g., Lai et al. 1993). Note that $\bar{\mathcal{C}} = \mathcal{C}/\sqrt{GM^3R_0}$ is an adimensional quantity, $\mathcal{C} = -(k_nMC)/(5\pi)$ has the dimensions of an angular momentum, and both are proportional to the conserved circulation C. It can be shown that (Lai & Shapiro 1995)

$$\mathcal{C} = I\Lambda - \frac{2}{5}k_nMa_1a_2\Omega, \tag{10}$$

where $I = k_nM(a_1^2 + a_2^2)/5$ is the NS moment of inertia with respect to the rotational axis. Along the secular equilibrium sequence, we write the NS spin-down law as (Shapiro & Teukolsky 1983)

$$\frac{dE}{dT} = -\frac{B_p^2R^6\Omega_{\rm eff}^4}{6c^3} - \frac{32GI^2\epsilon^2\Omega^6}{5c^5} = L_{\rm dip} + L_{\rm GW}, \tag{11}$$

where E is the NS total energy, $L_{\rm GW} = dE_{\rm GW}/dT$ accounts for GW losses, while $L_{\rm dip} = dE_{\rm dip}/dT$ for magnetic dipole ones. Here $\epsilon = (a_1^2 - a_2^2)/(a_1^2 + a_2^2)$ is the ellipticity, B_p is the dipolar field strength at the poles, Ω is the pattern angular frequency *of*

[6] In the ellipsoidal approximation, surfaces of constant density are assumed to be self-similar ellipsoids, so the geometry of the configuration is completely specified by the three principal axes a_1, a_2 and a_3, and the axis ratio a_3/a_1 and a_2/a_1 are the same for all interior isodensity surfaces (Lai et al. 1993).

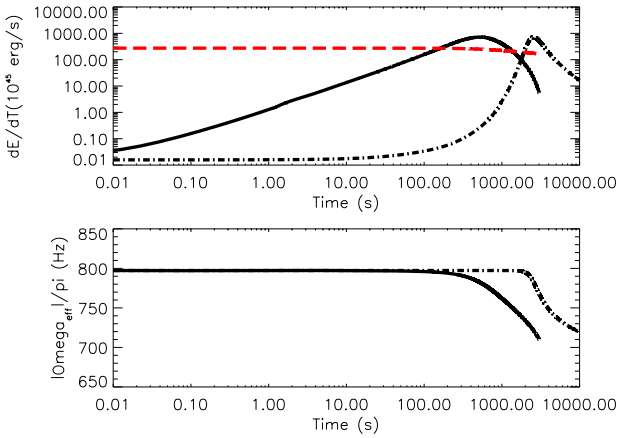

Figure 2. NS evolution along a Riemann-S sequence with parameters $(\bar{\mathcal{C}}, n, M, R_0, B_{p,0}) = (-0.41, 1, 1.4\ M_\odot, 20\ \mathrm{km}, 10^{14}\ \mathrm{G})$. Upper panel: the rate of energy loss in units of 10^{45} erg s^{-1}, when both magnetic dipole losses (red-dashed line) and GW losses (black-solid line) are taken into account in the magnetar's spin-down law. For reference, we also plot the rate of energy loss in the case only GW emission is considered (black-dash-dotted line), as in Lai & Shapiro (1995). Lower panel: the absolute value of the surface fluid particles angular frequency divided by a factor of π (i.e., $|\Omega_{\rm eff}|/\pi$), when both magnetic dipole and GW losses are considered (black-solid line). For reference, we also plot the same quantity when only GW losses are taken into account in the magnetar's spin-down law (black-dash-dotted line), as in Lai & Shapiro (1995). Note that the vertical axis in the lower panel is a linear scale: between 10^2 s and $\sim 10^3$ s, $\Omega_{\rm eff}/\pi$ changes from ~800 Hz to ~750 Hz, i.e., less than ~10% of its initial value. Thus, between 10^2 s and 10^3 s the power-law approximation to dipole losses is $L_{\rm dip} \propto T^{-0.11}$, so that $q \sim 0$ can be assumed for $T \lesssim 10^3$ s.

(A color version of this figure is available in the online journal.)

the ellipsoidal figure, R is the *mean stellar radius*, c is the light speed, and T is the time measured in an inertial frame where the pulsar is at rest. $L_{\rm dip}$ is computed conserving the magnetic field flux over a sphere of radius equal to the mean stellar radius (i.e., $B_p R^2 = \mathrm{const} = B_{p,0} R_0^2$ along the sequence, where R is the geometrical mean of the ellipsoid principal axes), and using the effective angular frequency $\Omega_{\rm eff}$, which includes both the pattern speed and the effects of the internal fluid motions. The use of $\Omega_{\rm eff} = \langle\Omega_0\rangle = \left\langle \frac{1}{r_\perp} |\widehat{r}_\perp \times \vec{u}_0| \right\rangle$ accounts for the fact that in the frozen-in magnetic field approximation (see e.g., Goldreich & Julian 1969; Baym et al. 1969; Thompson & Duncan 1996; Morsink & Rezania 2002; Thompson et al. 2002) the magnetic field lines are in effect tied to the fluid particles on the stellar surface. Note that $\Omega_{\rm eff}$ (and the corresponding dipole loss term) is measured in the inertial frame, which is where we compute dE/dT as well.

Once $(\bar{\mathcal{C}}, n, M, R_0, B_{p,0})$ are assigned, each configuration along a constant-$\bar{\mathcal{C}}$ sequence is completely determined specifying the axis ratio $x = a_2/a_1$ in the ellipsoid equatorial plane. Thus, all relevant quantities can be considered as functions of x only, and Equation (11) can be written as

$$\frac{dx}{dT} = \frac{L_{\rm dip}(x) + L_{\rm GW}(x)}{dE/dx}. \quad (12)$$

We solve the above equation numerically, with its right-hand side evaluated along a constant-$\bar{\mathcal{C}}$ Riemann-S sequence, and imposing an initial condition sufficiently near to a uniformly rotating Maclaurin spheroid, $(x(t_i) = x_i \to 1)$ of the given circulation $\bar{\mathcal{C}}$.

6. RESULTS AND DISCUSSION

In Figure 2, we compare the luminosity emitted in GWs, computed with (black-solid line) or without (black-dash-dotted line) the addition of the dipole loss term (red-dashed line) in Equation (11), for a typical choice of parameters, $(\bar{\mathcal{C}}, n, M, R_0, B_{p,0}) = (-0.41, 1, 1.4\ M_\odot, 20\ \mathrm{km}, 10^{14}\ \mathrm{G})$. Note that $\bar{\mathcal{C}} = -0.41$ corresponds to a value of $\beta = 0.20$ for the initial Maclaurin configuration, i.e., in the middle of the $0.14 < \beta < 0.27$ range for the secular instability. As evident from the lower panel of Figure 2, as long as the circulation is conserved, $\Omega_{\rm eff}$ remains nearly constant during all the evolution, and $|L_{\rm dip}| \sim 3 \times 10^{47}$ ergs s^{-1} $= L_0$ (upper panel, red-dashed line). As underlined in Section 2, energy pumped into the fireball at a constant rate is sufficient to explain the observed temporal behavior of afterglow plateaus (i.e., $\alpha \gtrsim -0.5$; see Figure 1). For what concerns the duration of the plateau, for a GRB with impulsive isotropic energy of the order of $E_{\rm imp} \sim 10^{50}$ ergs, the effect of the energy injection in the light curve will become visible after a time $T_c \sim E_{\rm imp}/L_0 \sim (10^{50}\mathrm{ergs})/(3 \times 10^{47}\ \mathrm{erg\ s^{-1}}) \sim 300$ s (see the red-dashed line in Figure 2 and Section 3), which is about in the middle of the observed range for $T_{\rm break,1} \sim$ 100–500 s (see Figure 1). Assuming the energy injection ends or starts fading significantly when the star approaches the final Dedekind state (see the discussion at the end of this section), the GRB light curve will return to its standard behavior after $T_{\rm break,2} \gtrsim 10^3$ to be compared with the observed range of $10^3 - 10^4$ s. Thus, for a GRB with such impulsive energy, the properties of the plateau associated with the NS secular evolution are in agreement with those typically observed.[7]

The waveform of the GW signal emitted in association with the afterglow plateau is computed as (Lai & Shapiro 1995)

$$h_+ = -\frac{h(t)}{2}\cos\Phi(1+\cos^2\theta) h_\times = -h(t)\sin\Phi\cos\theta, \quad (13)$$

where θ is the angle between the line of sight and the rotation axis of the star, $\Phi = 2\int_{t_0}^{t} \Omega t$ is twice the orbital phase, and

$$h(t) = \sqrt{\left(\frac{2c^3 d^2 \Omega^2}{5G}\right)^{-1} |L_{\rm GW}|} = \frac{4G\Omega^2}{c^4 d} I\epsilon, \quad (14)$$

where d is the distance to the source, $L_{\rm GW}$ and Ω are shown in Figures 2 (upper panel, black-solid line) and 3 (lower panel, black solid line), respectively. The resulting GW signal is quasi-periodic, with frequency $f = \Omega/\pi$.

To estimate the GW signal detectability, we proceed as follows. For broadband interferometers such as LIGO and VIRGO, the best signal-to-noise ratio is obtained by applying a matched filtering technique to the data, when a waveform template is available. In such a case,

$$\rho^2 = 4\int_0^{+\infty} \frac{(F_+^2 |\widetilde{h}_+(f,\theta)|^2 + F_\times^2 |\widetilde{h}_\times(f,\theta)|^2)}{S_h(f)} df, \quad (15)$$

where $\widetilde{h}$ is a Fourier transform, $S_h(f)$ is the power spectral density of the detector noise, F_+, $F_\times$ are the beam pattern functions ($0 < F_+^2, F_\times^2 < 1$ depending on the source position in the sky; see e.g., Thorne 1987; Flanagan & Hughes 1998). For the signal in Equation (13), in the stationary phase approximation (Thorne 1987; Cutler & Flanagan 1994; Owen et al. 1998; Owen & Lindblom 2002),

$$\rho^2 = \int_0^{+\infty} \frac{h^2(t)(dt/df)(F_+^2(1+\cos^2\theta)^2/4 + F_\times^2\cos^2\theta)}{S_h(f)} df. \quad (16)$$

[7] Note that in our discussion we are neglecting redshift effects, since we are interested in nearby GRBs at $z \lesssim 0.035$, i.e., having luminosity distances $d_L \lesssim 150$ Mpc.

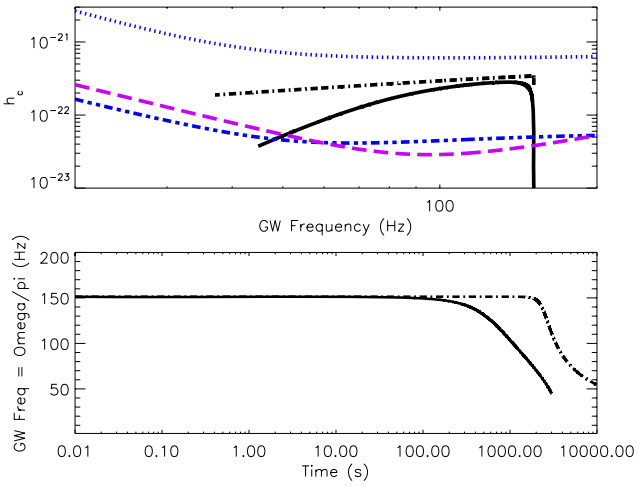

Figure 3. Upper panel: characteristic GW amplitude h_c at $d = 100$ Mpc, with dipole plus GW (black-solid line) and only GW (black-dash-dotted line, see also Lai & Shapiro 1995) losses being considered. A typical fit to the sensitivity expected for advanced detectors (purple-dashed line; see e.g., Cutler & Flanagan 1994; Owen et al. 1998), Virgo nominal sensitivity (blue-dotted line), and the advanced Virgo sensitivity optimized for binary searches (blue-dash-dot-dotted line; Acernese et al. 2008b), are also shown. Lower panel: evolution of the GW signal frequency, with dipole plus GW (black-solid line) and only GW (black-dash-dotted line) losses being considered in the NS spin down.

(A color version of this figure is available in the online journal.)

Since we expect to observe the GRB on-axis, $\theta \simeq 0$. In the case of optimal orientation,

$$\rho^2_{\rm max} = \int_0^{+\infty} \frac{f^2 h^2(t)(dt/df)}{f S_h(f)} d(\ln f) = \int_0^{+\infty} \left(\frac{h_c}{h_{\rm rms}}\right)^2 d(\ln f), \quad (17)$$

being $h_c = f h(t)\sqrt{dt/df}$ the characteristic amplitude, and $h_{\rm rms} = \sqrt{f S_h(f)}$. In the upper panel of Figure 3, we compare h_c computed for a GRB at $d = 100$ Mpc, with the $h_{\rm rms}$ expected for the advanced detectors (Acernese et al. 2008b; Cutler & Flanagan 1994; Owen et al. 1998), for which $\rho_{\rm max} \gtrsim 5$ at $d \lesssim 100$ Mpc, or $d \lesssim 150$ Mpc if we make the assumption that knowledge of the GRB trigger time reduces the detection threshold, of a factor which as a rule of thumb we take equal to 1.5 (Kochanek & Piran 1993; Cutler & Thorne 2002). Higher confidence in an eventual detection may require $\langle\rho\rangle_{\rm sky} = \sqrt{2/5}\rho_{\rm max} \gtrsim 5$ in each of a three-detectors network with similar $h_{\rm rms}$ (Cutler & Flanagan 1994). With the help of the GRB trigger time roughly compensating the factor of $\sqrt{2/5}$, this implies $d \lesssim 100$ Mpc.

BATSE results show that about 3% of short GRBs are expected to be within 100 Mpc (Nakar et al. 2006), which translates into ∼1–2 short GRBs per year in the Swift (∼10 short GRBs per year) plus GBM (GLAST—∼1/4 of ∼200 GRBs per year) sample. As far as low-luminosity long GRBs, two of them (980425 and 060218) were already observed at a $d \sim 40$ Mpc and $d \sim 130$ Mpc, and their local rate ($\gtrsim$200 Gpc^{-3} yr^{-1}) is expected to be much higher than that of normal bursts (1 Gpc^{-3} yr^{-1}; e.g., Virgili et al. 2009). INTEGRAL has detected a large proportion of faint GRBs inferred to be local (Foley et al. 2008), a sample which may be increased by future missions such as Janus (Stamatikos et al. 2009) and EXIST.[8] To compare with the case discussed here, the standard progenitor scenario for *long* GRBs predicts $\rho \sim 5$ at 27 Mpc for the advanced Virgo/LIGO, while the chirp signal from *short* GRBs is estimated to be detectable up to several hundreds Mpc (e.g., Flanagan & Hughes 1998; Kobayashi & Mészáros 2003). GWs eventually detected after a chirp and during an electromagnetic plateau of a short GRB, would add a significant piece of information, probing whether a magnetar is formed in the coalescence, rather than a BH.

It is finally worth adding some few considerations more. First, in the scenario we are proposing here, some correlations do exist between the electromagnetic plateau and the GW signal, that could be explored in future analyses so as to test up to which level those may help the GW signal search. For example, a measurement of the initial frequency of the GW signal, for a given NS mass and radius, would allow one to derive an estimate $\beta_{\rm GW}$ for the actual value of β (see also Figure 5 in Lai & Shapiro 1995). In the ellipsoidal approximation, $\beta_{\rm GW}$ would predict a specific evolution of the bar, as e.g., the expected value of $\Omega_{\rm eff}(\beta_{\rm GW}) = \Omega(\beta_{\rm GW}) - \Lambda(\beta_{\rm GW})$ during the nearly constant phase. At the same time, the luminosity of the afterglow plateau, for a given NS mass, radius and magnetic field strength, would also allow one to estimate the value of $\Omega_{\rm eff}$ during the constant phase, which could thus be checked for consistency with the value $\Omega_{\rm eff}(\beta_{\rm GW})$ inferred from the GW measurements.

Next, some considerations are required on the fate of the bar after the final Dedekind state is reached. In the absence of dipole losses, the evolution of the NS along the sequence would have maintained Ω nearly constant up to a time $T_{\rm GW}$, of the order of few secular growth times, $\tau_{\rm GW} \simeq 2 \times 10^{-5}$ s $[M/(1.4\ M_\odot)]^{-3}\,[R_0/(10\ {\rm km})]^4\,(\beta - \beta_{\rm sec})^{-5}$ (Lai & Shapiro 1995). Here β is referred to the initial Maclaurin configuration, and it is determined by the choice of $\bar{C}$. In our case, $\bar{C} = -0.41$ and $\beta = 0.20$, so that $\tau_{\rm GW} \simeq 335$ s. As evident from the black-dash-dotted line in the lower panel of Figure 3, for such value of the circulation, when only GW losses are considered, one has $T_{\rm GW} \simeq (1\text{–}2) \times 10^3$ s $\simeq (3\text{–}6)\tau$. The addition of magnetic dipole losses speeds up the process, so that the star reaches the stationary football configuration somewhat earlier (Figure 3, lower panel, black-solid line). After the end of the secular evolution, we do not know what the fate of the bar is. As Lai & Shapiro (1995) have underlined, while the star approaches a Dedekind ellipsoid the gravitational evolution timescale increases, eventually becoming comparable to the viscous dissipation one. When this happens, $\bar{C}$ is no longer conserved and the star is expected to be driven along a nearly Dedekind sequence to become a Maclaurin spheroid, since this is the only final state that does not radiate GWs or dissipate energy viscously. The addition of magnetic dipole losses would speed up such evolution, and further spin-down the final Maclaurin state. We thus expect to have $\Omega_{\rm eff}$ decreasing at some point after the constant$-\bar{C}$ evolution, with the dipole luminosity $L_{\rm dip}$ also decreasing accordingly. Correspondingly, the energy injected into the fireball will start decreasing (eventually entering in the $q < -1$ phase, see Section 2), and the afterglow plateau is expected to end, with the light curve turning back to the temporal decay expected in the absence of continuous energy injection. In view of these considerations, and for the purpose of this paper, we have limited our discussion to show that the properties of the electromagnetic plateau, even assuming this suddenly ends after the constant$-\bar{C}$ evolution, are in agreement with those typically observed in GRBs.

[8] http://exist.gsfc.nasa.gov/

7. CONCLUSION

We have discussed a possible scenario where a newly formed magnetar is left over after a GRB explosion, and explored the hypothesis of its being subject to a secular bar-mode instability, including in the spin down the contributions of both radiative losses by magnetic dipole emission and by GWs. Following the analytical treatment of Lai & Shapiro (1995), we have shown that for reasonable values of the physical parameters, the typical properties of GRB afterglow X-ray plateaus may be reproduced. A consequence of this is that, on the relatively long timescale 10^3–10^4 s of the electromagnetic plateau, the advanced LIGO/Virgo interferometers may detect a corresponding GW signal up to $d \sim 100$ Mpc by carrying out matched searches. Such a signal would be associated with an afterglow light-curve plateau from a long subluminous GRB, or from a short GRB, with isotropic energy $\lesssim 10^{50}$ erg, which is typical of most nearby GRBs detected. For the more energetic GRBs, a bar-mode GW signal may be detected without a visible plateau in the afterglow.

In conclusion, although there are considerable uncertainties about the evolutionary path of newborn magnetars, our analysis indicates that the scenario proposed here is a plausible and interesting possibility, leading to an efficient GW emission process which is accompanied by a distinctive electromagnetic signature. Thus, in view of the impending commissioning of the advanced LIGO and Virgo, we consider that it would be highly worth testing this possibility through matched electromagnetic-GW data searches.

We thank Benjamin Owen for important comments and valuable suggestions on this scenario, and for helping improve the manuscript. A.C. thanks Fulvio Ricci for crucial support during this project, Giovanni Montani for important discussions, Cristiano Palomba for very helpful suggestions, and Christian D. Ott for useful comments. This work was supported by the "Fondazione Angelo della Riccia"-bando A.A. 2007–2008 & 2008–2009 (A.C.), and by NSF PHY-0757155 & NASA NNX08AL40G (P.M.). A.C. gratefully acknowledges the support of the Penn State Institute for Gravitation and the Cosmos (IGC).

REFERENCES

Abbott, B., et al. 2008a, Phys. Rev. D, 77, 062004
Abbott, B., et al. 2008b, ApJ, 681, 1419
Acernese, F., et al. 2008a, Class. Quantum Grav., 25, 225001
Acernese, F., et al. 2008b, AdV Prelimiary Design, VIR-089A-08
Andersson, N. 1998, ApJ, 502, 708
Andersson, N. 2003, Class. Quantum Grav., 20, 105
Andersson, N., & Kokkotas, K. D. 2001, Int. J. Mod. Phys. D, 10, 381
Arons, J. 2003, ApJ, 589, 871
Baiotti, L., et al. 2007, Phys. Rev. D, 75, 044023
Baym, G., et al. 1969, Nature, 224, 674
Blackman, E. G., & Yi, I. 1998, ApJ, 498, L31
Bondarescu, R., et al. 2009, Phys. Rev. D, 79, 104003
Bucciantini, N., et al. 2009, MNRAS, 396, 2038
Burrows, A., & Hayes, J. 1996, Phys. Rev. Lett., 76, 352
Centrella, J. M., et al. 2001, ApJ, 550, L193
Chandrasekhar, S. 1939, An Introduction to the Study of Stellar Structure (Chicago, IL: Chicago Univ. Press)
Chandrasekhar, S. 1969, Ellipsoidal Figures of Equilibrium (New Haven, CT: Yale Univ. Press)
Chandrasekhar, S. 1970, Phys. Rev. Lett., 24, 611
Cutler, C. 2002, Phys. Rev. D, 66, 084025
Culter, C., & Flanagan, E. E. 1994, Phys. Rev. D, 49, 2658
Cutler, C., & Thorne, K. S. 2002, in 16th Int. Conf. on Genral Relativity and Gravity, ed. N. T. Bishop & D. M. Sunil (Singapore: World Scientific), 72
Dai, Z. G., & Lu, T. 1998, A&A, 333, 87
Dall'Osso, S., & Stella, L. 2007, Ap&SS, 308, 119
Dall'Osso, S., Shore, S. N., & Stella, L. 2008, MNRAS, in press (arXiv: 0811.4311D)
Di Matteo, T., Perna, R., & Narayan, R. 2002, ApJ, 579, 706
Dimmelmeir, H. 2008, Phys. Rev. D, 78, 064056
Duncan, R. C., & Thompson, C. 1992, ApJ, 392, L9
Epstein, R. 1978, ApJ, 223, 1037
Fan, Y.-Z., & Dong, X. 2006, MNRAS, 372, 19
Flanagan, E. E., & Hughes, S. A. 1998, Phys. Rev. D, 57, 4535
Foley, S., et al. 2008, A&A, 484, 143
Friedman, J. L., & Morsink, S. 1998, ApJ, 502, 714
Friedman, J. L., & Schutz, B. F. 1978, ApJ, 222, 281
Goldreich, P., & Julian, W. H. 1969, ApJ, 157, 869
Ho, W. C. H., & Lai, D. 2000, ApJ, 543, 386
Kluzniak, W., & Ruderman, M. 1998, ApJ, 505, L113
Kobayashi, S., & Mészáros, P. 2003, ApJ, 589, 861
Kochanek, C. S., & Piran, T. 1993, ApJ, 417, L17
Kokkotas, K. D. 2008, Rev. Mod. Astrophys., 20, 140
Lai, D. 2001, in AIP Conf. Proc. 575, Astrophysical Sources for Ground-based Gravitational Wave Detectors, ed. J. M. Centrella (Melville, NY: AIP), 246
Lai, D., Rasio, F. A., & Shapiro, S. L. 1993, ApJS, 88, 205
Lai, D., & Shapiro, S. L. 1995, ApJ, 442, 259
Lee, W. H., et al. 2005, ApJ, 632, 421
Levan, A. J., et al. 2006, MNRAS, 368, 1
Lindblom, L., & Owen, B. J. 2002, Phys. Rev. D, 65, 063006
Lindblom, L., et al. 1998, Phys. Rev. Lett., 80, 4843
MacFadyen, A. I., & Woosley, S. E. 1999, ApJ, 524, 262
Manca, G. M., et al. 2007, Class. Quantum Grav., 24, S171
Mazzali, P. 2006, Nature, 442, 1018
Mereghetti, S. 2008, A&A Rev., 15, 225
Mészáros, P., & Rees, M. J. 1997, ApJ, 476, 232
Morsink, S. M., & Rezania, V. 2002, ApJ, 574, 908
Müller, E., & Janka, H. T. 1997, A&A, 317, 140
Müller, E., Rampp, M., Buras, R., & Janka, H.-T. 2004, ApJ, 603, 221
Nakamura, T. 1998, Prog. Theor. Phys., 100, 921
Nakar, E., et al. 2006, ApJ, 650, 281
Nousek, J. A., et al. 2006, ApJ, 642, 389
Oechslin, R., & Janka, H.-T. 2006, MNRAS, 368, 1489
Ott, C. D., et al. 2005, ApJ, 625, L119
Ou, S., et al. 2004, ApJ, 617, 490
Owen, B. J., & Lindblom, L. 2002, Class. Quantum Grav., 19, 12470
Owen, B. J., et al. 1998, Phys. Rev. D, 58, 4020
Palomba, C. 2000, A&A, 354, 163
Panaitescu, A. 2008, MNRAS, 383, 1143
Panaitescu, A. 2009, in AIP Conf. Ser. 1133, Gamma-ray Burst: Sixth Huntsville Symp., ed. C. Meegan, C. Kouveliotou, & N. Gehrels (Melville, NY: AIP), 127
Panaitescu, A., & Vestrand, W. T. 2008, MNRAS, 387, 497
Panaitescu, A., et al. 2006, MNRAS, 369, 2059
Popham, R., et al. 1999, ApJ, 518, 356
Racusin, J., et al. 2008, Nature, 455, 183
Rezzolla, L., et al. 2001, Phys. Rev. D, 64, 104014
Ruderman, M., Tao, L., & Kluz′niak, W. 2000, ApJ, 542, 243
Sari, R., & Piran, T. 1999, ApJ, 520, 641
Sari, R., Piran, T., & Narayan, R. 1998, ApJ, 497, L17
Saijo, M., et al. 2002, ApJ, 595, 352
Shapiro, S. L., & Teukolsky, S. A. 1983, Black Hole, White Dwarfs, and Neutron Stars: The Physics of Compact Objects (New York: Wiley)
Shibata, M., & Karino, S. 2004, Phys. Rev. D, 70, 4022S
Shibata, M., & Sekiguchi, Y. 2005, Phys. Rev. D, 71, 024014
Soderberg, A. M., et al. 2006, ApJ, 650, 261
Spruit, H. C. 1999, A&A, 341, L1
Stamatikos, M., et al. 2009, Contributed to the SSE-SFP of the Astro2010 Decadal Survey (arXiv:0902.3022S)
Stella, L., et al. 2005, ApJ, 634, L165
Thompson, C. 1994, MNRAS, 270, 480
Thompson, C., & Duncan, R. C. 1996, ApJ, 473, 322
Thompson, C., Lyutikov, M., & Kulkarni, S. R. 2002, ApJ, 574, 332
Thorne, K. S. 1987, 300 Years of Gravitation (Cambridge: Cambridge Univ. Press), 330
Usov, V. V. 1992, Nature, 357, 472
Virgili, F. J., et al. 2009, MNRAS, 392, 91
Wheeler, J. C., et al. 2000, ApJ, 537, 810
Yi, I., & Blackman, E. G. 1998, ApJ, 494, L163
Yu, Y., & Huang, Y.-F. 2007, Chin. J. Astron. Astrophys., 7, 669
Zhang, B., & Mészáros, P. 2001, ApJ, 552, 35
Zhang, B., et al. 2006, ApJ, 642, 354
Zhang, D., & Dai, Z. G. 2009, ApJ, submitted (arXiv:0901.0431v1)